Lidar profiles of fish schools

James H. Churnside, James J. Wilson, and Viatcheslav V. Tatarskii

A lidar system was used in a seawater tank to measure the average diffuse reflectivity of live sardines. Diffuse reflectivity was measured to be 10% for a copolarized laser return and 3% for a cross-polarized return. We used these calibration measurements to infer the density of sardines in areas of the Southern California Bight from vertical profiles obtained with the lidar mounted on a ship. Within schools densities up to ~ 0.01 kg m^{-3} were observed. During hourly survey periods total habitat densities up to $\sim 2 \times 10^{-3}$ kg m^{-2} were observed.

1. Introduction

Direct biomass surveys are an important tool for fishery research and stock assessment. Biomass survey data are used in stock assessments, along with data on fishing effort and age composition of landed fish, to determine stock size, productivity, and sensitivity to fishing. The use of biomass surveys is increasing as resources become fully utilized and require frequent and accurate monitoring for proper management. The traditional direct surveys—ichthyoplankton, acoustic, and trawl—have substantial limitations when applied to active epipelagic fishes such as mackerels, sardines, anchovies, and menhaden because of the time and cost associated with sampling even a small fraction of the habitat with surface vessels. In addition, schooling fishes may avoid surface vessels and sampling nets, leading to possible bias in some surveys.[1] This suggests that aerial surveys would be a valuable supplement to traditional techniques. Visual observations from aircraft have been used in stock assessment; however, visual observations are limited to shallow schools under favorable conditions.

It was observed some time ago that fish could be detected by use of airborne lidar,[2] and several attempts have been made to model the performance of such a system.[3,4] To test the performance of a lidar system under more controlled conditions than those of previous experiments, we installed one on the flying bridge of the Research Vessel (R/V) *David Starr Jordan* and operated it for 3 weeks in the Southern California Bight. The ship's echo sounder was also operated during this time to provide a comparison with acoustic data.

Obtaining calibrated estimates of fish populations from lidar signals requires knowledge of the reflectivity of fish. Squire and Krumboltz[2] assumed a reflectivity of 50% when estimating the area of the fish intercepted by a lidar. Krekova *et al.*[3] followed Murphree *et al.*[4] in assuming a reflectivity of 5% for modeling purposes. Fredriksson *et al.*[5] measured the lidar return from dead fish, but their system was not calibrated. Churnside and McGillivary[6] made calibrated measurements of dead fish and obtained reflectivities of 18–26% in the blue portion of the spectrum and 15–22% in the green, depending on species. These values assume uniform reflection into 2π sr; the equivalent Lambertian reflectivities (into π sr) are actually half these values. Benigno and Kemmerer[7] measured the reflectivity of menhaden in the water at $<1\%$ across the blue-green portion of the spectrum by use of natural light. To calibrate our lidar system we measured the reflectivity of captive fish in a 10-m-deep tank.

We then mounted the same lidar on the flying bridge of the R/V *David Starr Jordan* and made open-ocean measurements of the returns from fish. We converted these returns to estimates of fish density by using the reflectivity measured in the tank experiment. Estimates of the average mass density of fish within the lidar beam can be obtained in this way if the mass per unit area of the fish is known. From the mass density within the lidar beam we can easily estimate the average mass density of a surveyed area.

J. H. Churnside and J. J. Wilson are with National Oceanic and Atmospheric Administration (NOAA) Environmental Technology Laboratory, 325 Broadway, Boulder, Colorado 80303. V. V. Tatarskii is with NOAA/University of Colorado, Cooperative Institute for Research in the Environmental Sciences, 325 Broadway, Boulder, Colorado 80303.

Received 26 September 1996; revised manuscript received 5 May 1997.

0003-6935/97/246011-10$10.00/0

Table 1. Lidar Transmitter and Receiver Parameters

Parameter	Value
Transmitter	
Wavelength	532 nm
Pulse length	15 ns
Pulse energy	67 mJ
Pulse repetition rate	10 Hz
Beam divergence	43 mrad
Receiver	
Aperture diameter	17 cm
Field of view	26 mrad
Optical bandwidth	10 nm
Electronic bandwidth	100 MHz
Sample rate	1 GHz

Table 2. Parameters of Fish in the Tank

Parameter	Mean	Standard Deviation
Sardine		
Weight (g)	39.3	7.4
Standard length[a] (cm)	14.8	7.6
Fork length[b] (cm)	16.0	8.4
Total length[c] (cm)	17.7	9.3
Anchovy		
Weight (g)	13.1	2.0
Standard length[a] (cm)	11.2	6.5
Fork length[b] (cm)	12.3	6.6
Total length[c] (*cm*)	13.4	7.1

[a]To beginning of tail.
[b]To fork of tail.
[c]To end of tail.

2. Apparatus

We used a coaxial, radiometric lidar in this research. The laser was a frequency-doubled, *Q*-switched Nd:YAG laser. The output was linearly polarized, and we equipped the laser with a half-wave plate to rotate the plane of polarization. The laser beam was diverged with a single plano–concave lens. The laser divergence was selected to ensure that the laser light reflected from the sea surface would not present an ocular hazard to personnel on the ship. We used a pair of mirrors to direct the beam so that the transmitter and receiver were coaxial. The pertinent transmitter and receiver parameters are listed in Table 1.

The receiver consisted of a refracting telescope that collected the returned signal onto a microchannel-plate detector. The field of view of the receiver was determined by the focal length of the lens and the diameter of the detector. It would have been desirable to increase this field of view to match the laser divergence, which would have required a shorter focal length lens, a larger detector area, or relay optics, but none of these options was practical. An interference filter in front of the detector limited the amount of background light that reached the detector. A rotatable polarizer in front of the filter allowed us to select the copolarized or the cross-polarized return. The detector output was fed directly into an amplifier with a logarithmic response. The log-amplifier output was digitized with an eight-bit digitizer, and the data were transferred to the computer and stored on optical disks.

The system was mounted on the flying bridge of the R/V *David Starr Jordan*, 10.3 m above the water and 4.3 m starboard of the center of the ship. The system was directed outward at an angle of 15° to put the beam beyond the ship wake. Generally, lidar profiles of fish schools were obtained with the laser polarized parallel to the plane of incidence to minimize reflection and the receiver cross polarized. This seemed to provide the best contrast between the background return from the water and fish returns.

3. Calibration Measurements

The same lidar was used for the calibration measurements, but two changes were made. First, the minimum range for the microchannel plate was too large for the tank experiment, so a photomultiplier tube was used. Second, the digitizer board malfunctioned, so the log-amplifier output was digitized with a digital oscilloscope, and then the data were transferred to the computer. Because the transfer rate was slow, only one laser pulse in 10 could be recorded. Data were recorded in 500-s blocks (i.e., 500 pulses recorded per block). Transmitter beam divergence and receiver field of view were not modified.

The system was placed on the edge of the deep tank at the Scripps Institution of Oceanography. This tank is ~3 m across and ~10 m deep. The lidar was pointed toward the center of the bottom of the tank at an angle of ~15° from vertical. The polarization was adjusted to be parallel to the plane of surface reflection. A 30-cm-diameter white disk was suspended just above the bottom of the tank. The laser beam, with an estimated diameter of 32 cm at a distance of 10 m, just covered the disk. The receiver field of view was slightly smaller, with a 20-cm diameter at the bottom of the tank. Data were collected with the receiver polarized in the same plane as the transmitter and also with it polarized in the orthogonal plane. A video camera was set up outside a window, ~2 m from the bottom of the tank. While the laser was operating, the shadows of the fish on the disk were recorded on videotape.

Live fish were placed in the tank ~2 weeks before the experiment to give them time to become accustomed to living in the tank. On the day of the experiment the tank contained ~480 sardines and 65 anchovies. Length and weight data are summarized in Table 2. The sardines were larger than the anchovies and tended to congregate closer to the surface. The fish did not seem to be affected by the laser beam. They did not try to avoid it and were not startled when it was turned on, even if they happened to be in the beam.

A typical lidar return from the tank has three

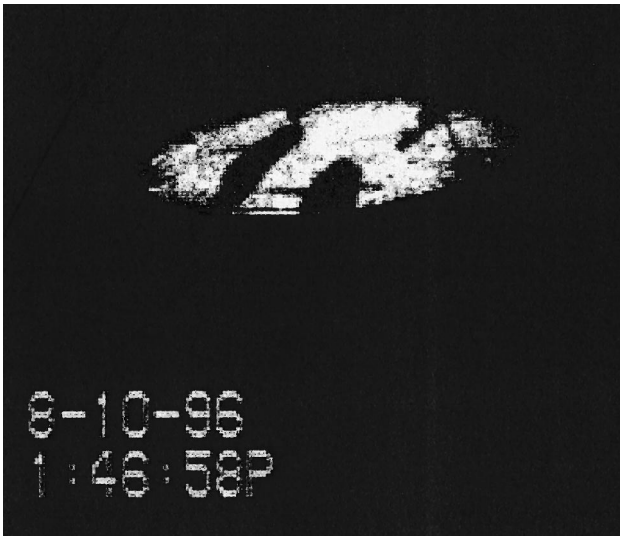

Fig. 1. Video of fish shadows on the bottom of the tank. (The year was set incorrectly; it should be 1995.)

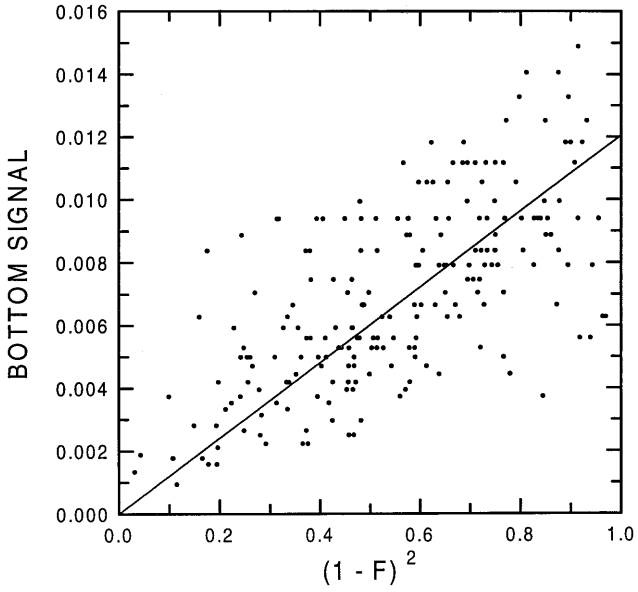

Fig. 2. Magnitude of the bottom signal as a function of $(1 - F)^2$ for the cross-polarized data set, where F is the fraction of the beam blocked by fish.

peaks, one from the surface, one from the fish, and one from the bottom. Each lidar return was examined. For those containing fish we recorded the depth of the fish return peak, the magnitude of the fish return peak, and the magnitude of the bottom return. Each of the logarithmic signal strengths was converted to an equivalent linear voltage across the 50-Ω load resistance.

The video frames corresponding to the lidar shots containing fish were also digitized. Figure 1 is a typical video image showing the time and date, the illuminated disk, and the shadows of fish. (The year was set incorrectly; it should read 1995.) The disk appears to be elliptical because it was recorded from the side of the tank. The section of each image containing the disk was selected and each pixel value was compared with a threshold to separate those portions of the disk image that contain fish from those that do not. From this the fraction of the disk that was covered by fish, F, was found. For the example shown, F was 29%. The transmission of light through the school is the fraction that is not blocked or $1 - F$.

We assume that the lidar signal from the disk, S_d, is proportional to the two-way transmission through the fish school:

$$S_d = C(1 - F)^2, \tag{1}$$

where C is a constant to be determined from the data.

Figure 2 shows, for the cross-polarized data set, a plot of the magnitude of the lidar signal from the bottom as a function of $(1 - F)^2$. These data are for the 210 lidar pulses where there were fish in the beam. Several factors that produce variations in the laser irradiance across the beam contribute to the scatter in the data. The laser-pulse energy fluctuates with a standard deviation of slightly less than 5%. Other sources include refraction at the surface and nonuniform scattering by particulates in the water. Another factor is that the receiver diameter and field of view were not identical to the laser beam diameter and divergence angle. Thus the fraction of the beam blocked on the return path was not identical to that on the path from the laser to the bottom target. This geometry was not ideal, but it was dictated by practical considerations. The solid line in Fig. 2 is a linear regression of the data, which provides a value for C of $1.20 \times 10^{-2} \pm 2.71 \times 10^{-4}$ V.

The signal from the fish can be expressed as

$$S_f = C \frac{R_f}{R_d} \frac{z_d^2}{z_f^2} \exp[-2\alpha(z_f - z_d)] F, \tag{2}$$

where R represents reflectivity, z represents depth, and α is the attenuation coefficient of the lidar signal in the water. Equation (2) assumes that all the fish in any pulse are at the same depth. We observed that they generally stayed within a layer <1 m thick, and this assumption is reasonable. A depth-corrected fish signal S can be obtained by correction of Eq. (2) for the effects of attenuation and geometric losses, with the result that

$$S = \frac{z_f^2}{z_d^2} \exp[2\alpha(z_f - z_d)] S_f. \tag{3}$$

We used a value of 0.066 m^{-1} for α; with this value there was no residual trend on the depth of the depth-corrected signal. This value is slightly larger than the seawater absorption coefficient value of 0.054 m^{-1} at this wavelength and is a reasonable value for filtered seawater.

Figure 3 is a plot of the depth-corrected fish signal for the cross-polarized configuration as a function of F. The linear regression, plotted as a solid line, has a slope of $3.24 \times 10^{-4} \pm 1.75 \times 10^{-5}$ V. Note that

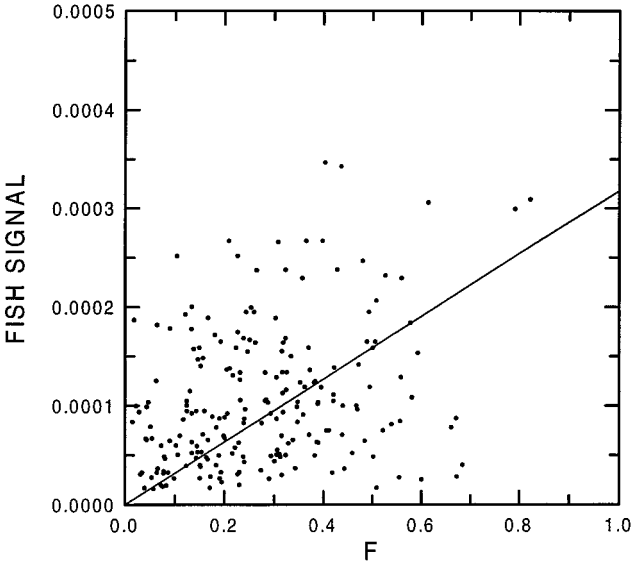

Fig. 3. Magnitude of the depth-corrected fish signal as a function of the fraction of the beam blocked by fish, F.

the scatter in the data from the fish is somewhat larger than that from the bottom. There are several reasons for this. If the fish within the beam are not all at the same depth, this will introduce some error in the depth-corrected signal. Fish that are within the beam area but shadowed by other fish do not affect the signal or the fraction of the area covered on the bottom of the tank. Thus these fish do not contribute to the scatter. However, fish that are outside the illuminated area but within the receiver field of view could block a portion of the light scattered from fish lower in the tank, and this would add to the scatter. This is probably not a large effect, because the fish were generally in a fairly thin layer. Also, the attenuation in the water may not be uniform from the top to the bottom of the tank.

However, most of the scatter is because of actual differences in the reflectivity. The reflectivity of individual fish will vary somewhat from one to another. It will also vary depending on the aspect angle of the fish. If a fish in the beam turns to expose its more reflective side, the reflected signal for that shot will be higher for the same fraction of the beam blocked than if all the fish in the beam are upright. The reflected signal will also depend on how normal the surfaces of the fish that are exposed to the illumination are, with more-normal surfaces contributing more signal. Despite these variations we can obtain an average reflectivity that should be valid in the open ocean, as long as the returns from many lidar pulses are used in a biomass estimate.

Using the values of the two slopes and Eq. (3), we obtain

$$R_f = \frac{3.24 \times 10^{-4} \pm 1.75 \times 10^{-5}}{1.20 \times 10^{-2} \pm 2.71 \times 10^{-4}} R_d. \tag{4}$$

The disk we used was not Lambertian. We measured the reflectivity of the disk in the laboratory at the same angle that was used in the tank and obtained a value of 0.360 ± 0.006 sr^{-1}. By combining all the uncertainties we arrived at a value for fish reflectivity of $9.72 \times 10^{-3} \pm 9.33 \times 10^{-4}$ sr^{-1}. If we compare a school of fish with a Lambertian reflector, we obtain an effective diffuse reflectivity of $3.1\% \pm 0.3\%$ for the cross-polarized data set.

For the copolarized data set there were fewer fish in the beam; only 42 of the lidar pulses contained clear fish returns. Part of the reason for this is that the scatter from the water was much higher in the copolarized lidar returns than in the cross-polarized data set, and the fish return was more difficult to see. However, the data were processed the same way as the cross-polarized set, starting with a plot (not presented here) of the bottom return as a function of $(1 - F)^2$ for this data set. The slope of these points was $1.22 \times 10^{-2} \pm 1.02 \times 10^{-3}$ V, which is very close to the value obtained for the cross-polarized data set. The fish data were treated as before, and the depth-corrected fish signal was plotted as a function of F. The slope in this case was $1.05 \times 10^{-3} \pm 1.17 \times 10^{-4}$ V. The larger relative uncertainty is because fewer lidar returns were available for averaging. The reflectivity was therefore $3.10 \times 10^{-2} \pm 6.54 \times 10^{-3}$ sr^{-1}. The diffuse reflectivity was $9.7\% \pm 2.1\%$.

The reflectivity for unpolarized light is the sum of the copolarized and cross-polarized values, so the diffuse reflectivity for unpolarized light would be $\sim$12.8%. This is slightly lower than the range of values measured when we used dead fish. The depolarization ratio is the ratio of the cross-polarization reflectivity to the copolarization reflectivity or $\sim$31%. This is within the range of values measured when we used dead fish. We observed that the fish were more visible in the cross-polarized lidar return.

4. Data Processing

The open-ocean data were acquired in the Southern California Bight with the lidar installed on a ship. Figure 4 is a plot of the logarithm of the lidar signal as a function of depth for a typical lidar pulse with no fish. The microchannel-plate detector was triggered to turn on when the lidar reached a depth of $\sim$5 m to avoid saturation of the detector by the surface return. The signal then decays nearly exponentially from its initial value to the background level, which is caused by background light reflecting into the receiver. The small peak at $\sim$10 m is a detector artifact that is a reflection of the trigger pulse. This peak was constant and easily removed from the final data product.

This type of lidar return can be approximated by use of the following equation:

$$S_w(z) = \frac{a \exp(-\alpha z)}{\left(nh \dfrac{\cos\theta_w}{\cos\theta_a} + z\right)^2} + b, \tag{5}$$

where S_w is the linear signal; a is an amplitude parameter that includes laser pulse energy, surface losses, receiver area, detector responsivity, etc., as

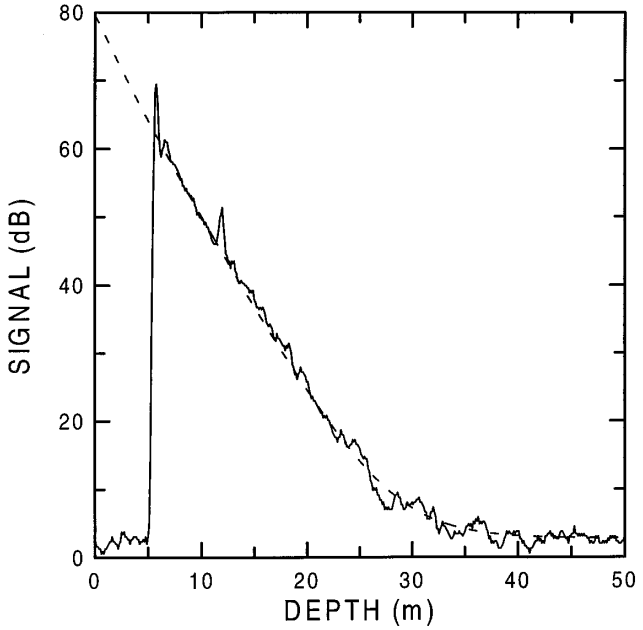

Fig. 4. Typical lidar return with no fish present. The dashed curve is a fit of the clear-water return.

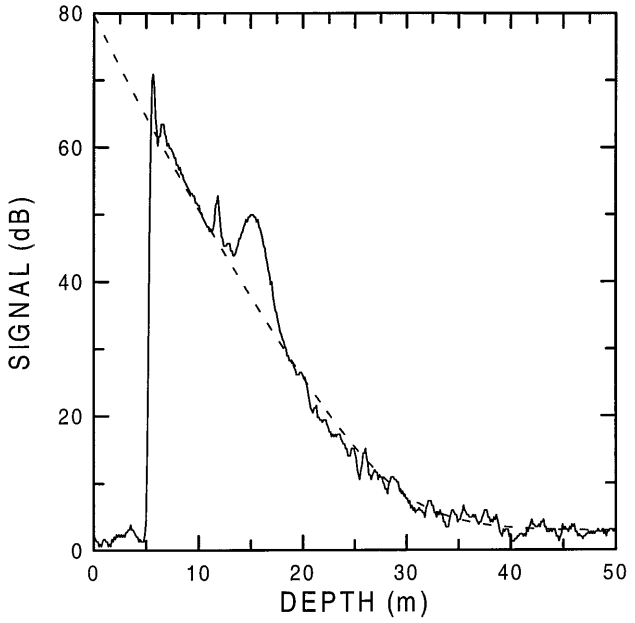

Fig. 5. Typical return from a lidar pulse that intercepts a school of fish at a depth of 15 m. The dashed curve is a fit of the clear-water return.

well as the backscatter coefficient of the water; α is the lidar attenuation coefficient; z is depth; h is the height above the surface; n is the index of refraction of water; θ_w is the angle between the beam in water and the surface normal; θ_a is the angle between the beam in air and the surface normal; and b is the background signal level. The angle in water is easily found from the angle in air by use of Snell's law.

Equation (5) contains the implicit assumption that the optical properties of the water are constant with depth. The dashed curve in Fig. 4 plots the values of Eq. (5), with a, α, and b chosen to match the data. The amplitude a for this case was 179 V m^2, while the background was 138 μV. The lidar attenuation coefficient was 0.116 m^{-1}. The agreement between the fitted curve and the measurements, typical of much of our data, suggests that the assumption of uniform optical properties is valid for this much of the area covered on this cruise.

If fish are present at some depth, there is an additional contribution to the signal at that depth, which depends on the backscatter coefficient of the fish, so

$$S(z) = a\left[1 + \frac{\beta_F(z)}{\beta_w}\right]\frac{\exp(-\alpha z)}{\left(nh\,\dfrac{\cos\theta_w}{\cos\theta_a} + z\right)^2} + b, \qquad (6)$$

where β_f and β_w are the backscatter coefficients of the fish and the water, respectively. The backscatter from fish is a function of depth for each pulse, but we have assumed that the attenuation of light by the fish can be neglected.

Figure 5 is a plot of the logarithm of a lidar pulse that contains a school of fish. The increase of the signal when fish are present is clear in the data. The dashed curve in Fig. 5 is an estimate of the clear-water return found by use of the same curve fit, with care taken so that depths where fish were present were not used. This pulse was selected from the same 1-min data file that contains the pulse selected for Fig. 4, and the parameters are very similar; the amplitude was 182 V m^2, the background was 139 μV, and the attenuation coefficient was 0.112 m^{-1}.

The data were processed in the following way. First, a, α, and b were estimated for each lidar pulse. We used these three parameters with Eq. (5) to obtain an estimate of the water return, $S_w(z)$. The background was subtracted linearly from both the signal and the estimated water return. Then the logarithm of the estimated water return was subtracted from the logarithm of the measured signal to obtain

$$\ln[S(z) - b] - \ln[S_w(z) - b] = \ln\left(1 + \frac{\beta_f(z)}{\beta_w}\right). \qquad (7)$$

From Eq. (7) we can obtain the ratio of the fish backscatter coefficient at each depth to the water backscatter coefficient, which is assumed to be independent of depth. It is given by

$$\frac{\beta_f(z)}{\beta_w} = \exp\{\ln[S_f(z) - b] - \ln[S_w(z) - b]\} - 1. \qquad (8)$$

Σ is defined by the right-hand side of Eq. (8) and is calculated from the signal. The backscatter ratio, on the left-hand side, is assumed to be proportional to the number of fish within the depth-resolution element.

One can obtain the backscatter coefficient of the water from the lidar signal, when no fish are present, by calibrating carefully the lidar against a standard target. To illustrate the technique, however, we use $\beta_w = 0.003$ m^{-1} sr^{-1}, which is a typical value for

unpolarized light in this region.[8] The depolarization of the lidar return was measured at 10 stations in the bight during this cruise. We use the average depolarization value of 5.25% here to estimate the backscatter coefficient of water when a cross-polarized lidar is used. The standard deviation of the depolarization measurements was 2.0%.

The fish backscatter coefficient β_f is the product of two components. The first is the effective Lambertian reflectivity of fish divided by π sr. The second is the fraction of the beam intercepted by fish per unit depth. This second quantity is also equivalent to the number of fish per unit volume times the average cross-sectional area of a single fish and to the biomass per unit volume times the average mass per unit cross-sectional area of the fish. Thus, if we know the average cross-sectional area of the fish, we can obtain an estimate of the number density. If we know the average mass per unit cross-sectional area, we can obtain the mass density. Laboratory measurements on sardines produced a value of $\sim$13 kg m^{-2} for the mass per unit area d.

For our case we can estimate the biomass density as

$$D = \frac{2\pi\beta_w d}{R_f} \sum = 0.21 \sum, \tag{9}$$

where the calibration factor was calculated from the parameters discussed above. D is in kilograms per cubic meter and is a function of depth. We find the mass per unit area of the ocean by integrating D over the depth range.

To illustrate the type of quantitative data that can be obtained from the lidar system, we calculated hourly distributions of fish density from the data. The background water signal was estimated and subtracted from each pulse return as described. A threshold level, determined by trial and error, was used to determine whether each pulse contained a fish return. The linearized signals from all pulses that contained fish during the hour were averaged. If the water column were exactly homogeneous, as was assumed, this average should represent the density of fish. In practice, there were inhomogeneities in the clear-water signal that could be observed in the shots that were determined not to contain fish. To eliminate this effect from the data, we used the average of the pulses with no fish present in each data file to correct the average fish return. The calibration factor presented in Eq. (9) was applied to the average corrected signal to produce an estimate of the density of fish within the pulses containing fish. Then the average fish density within schools was multiplied by the fraction of the number of pulses containing fish returns

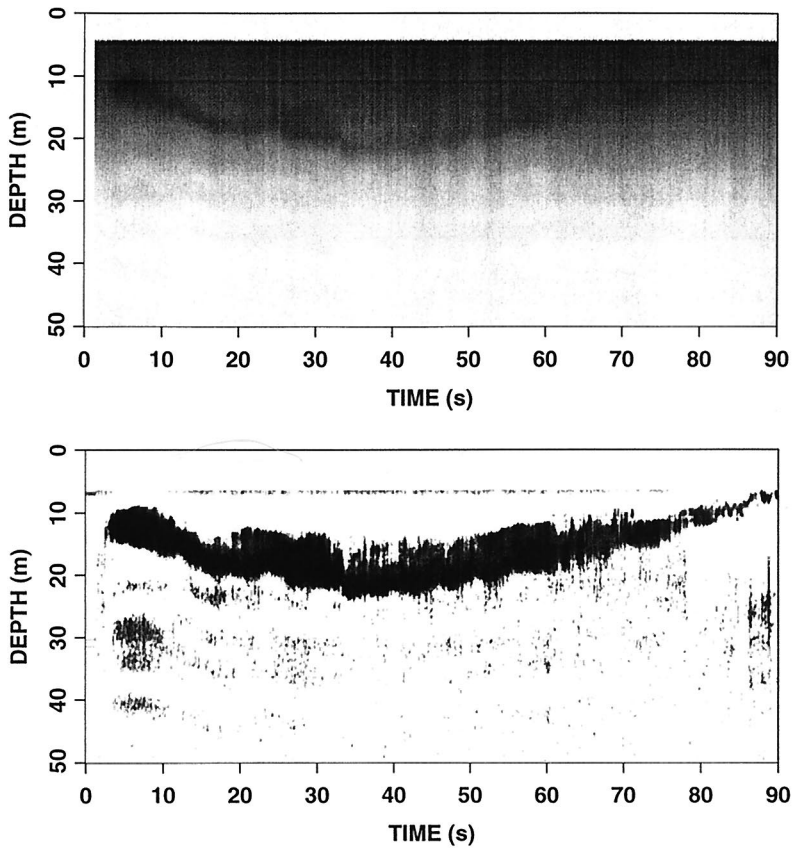

Fig. 6. Time–depth plot of lidar return from a school of fish, showing images of (top) raw data and (bottom) after both subtraction of the water return and contrast enhancement.

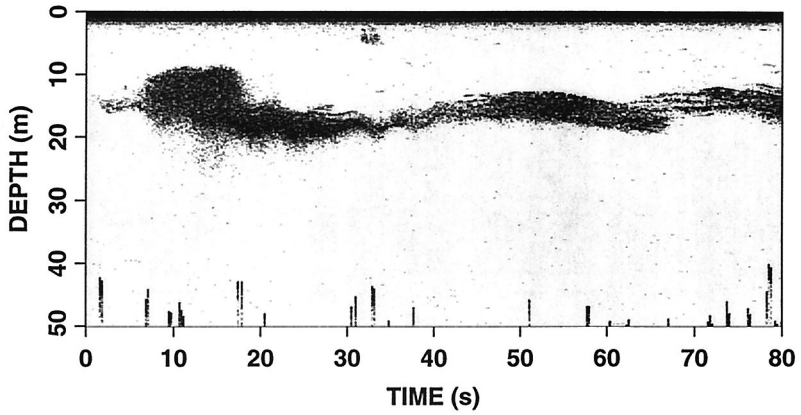

Fig. 7. Time–depth plot of the echo sounder record of the same school of fish as in Fig. 6.

within the hour to obtain an estimate of the density of fish within the habitat area surveyed during the hour.

5. Results

The top image in Fig. 6 is a plot of the log-amplifier output, represented as a gray scale, as a function of depth and of time, which is related to horizontal position through the ship's velocity. This image shows the data in raw form as they are displayed on the computer during operation. The bottom image in Fig. 6 shows the same data after removal of the clear-water return and after contrast enhancement. The depth, thickness, and temporal extent of the school of fish are clearly visible. Density variations within the school are also clear in the individual returns, although they are difficult to see in the high-contrast image. Figure 7 is an echo sounder image of the same school. Note the similarities in the size, shape, and depth of the school images obtained with the two instruments. The images are not identical because the instruments were not collocated.

We analyzed the fish density from the data taken on the morning of 24 September, 1995. The maximum density within schools obtained during this period was $\sim$0.01 kg m^{-3}. Since the density of fish is about the same as that of water, this implies that $\sim 10^{-5}$ of the volume within the school is occupied by fish. A sample trawl through the same area that evening produced $\sim$400 kg of sardines and small numbers of other fishes. These sardines had an average length of 0.159 m and an average mass of 0.0257 kg. From this we infer that the average vol-

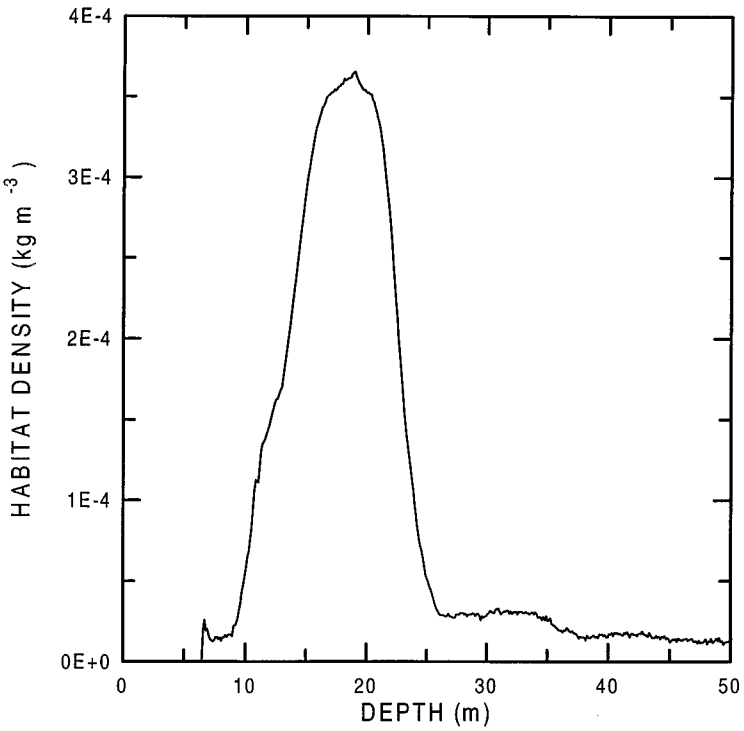

Fig. 8. Fish density for the habitat surveyed from 0600 to 0700 PDT, 24 September 1995.

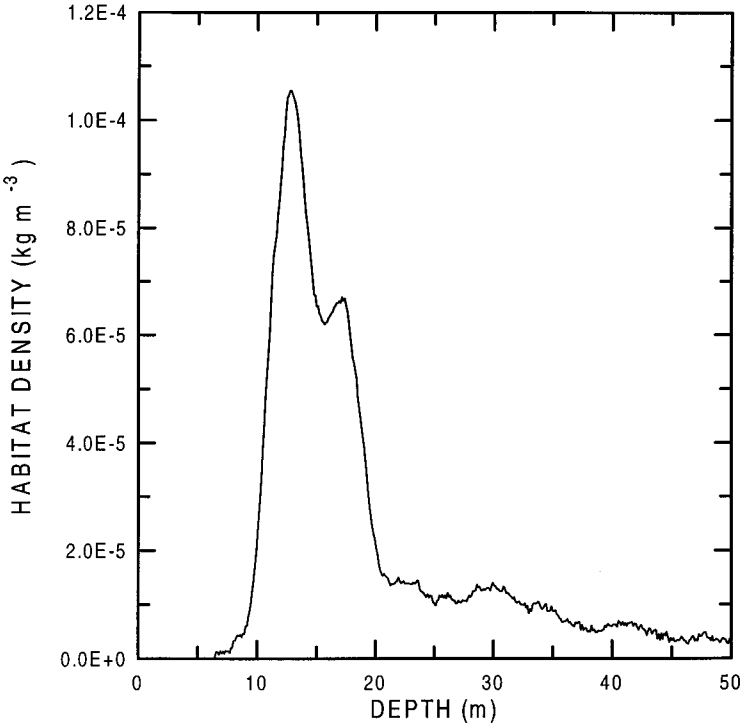

Fig. 9. Fish density for the habitat surveyed from 0700 to 0800 PDT, 24 September 1995.

ume of the fish was $\sim 6.39 \times 10^{-3} L^3$, where L is the average fish length. The maximum observed fish density was therefore about 1 fish in a volume of $\sim 639L^3$ or a separation of ~8.61 body lengths. Although fish packing density varies significantly, this is within the range of reported values.[8]

The average fish densities for each hour from 0600 to 0900 and from 1000 to 1100 Pacific Daylight Time (PDT) are presented in Figs. 8–11. From 0900 to 1000 PDT no fish returns were observed. During the first hour, 0600–0700 PDT, there was a broad layer of fish extending from ~10 to ~25 m deep.

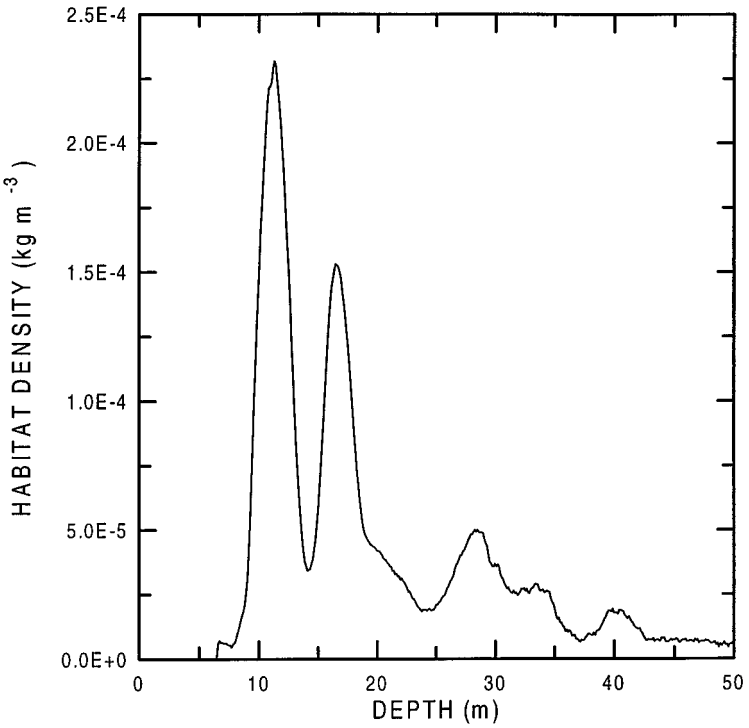

Fig. 10. Fish density for the habitat surveyed from 0800 to 0900 PDT, 24 September 1995.

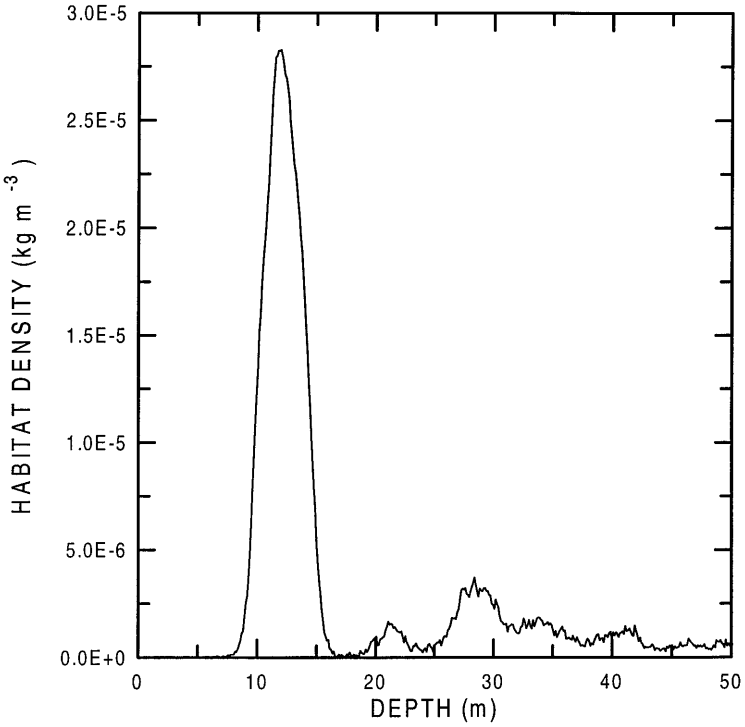

Fig. 11. Fish density for the habitat surveyed from 1000 to 1100 PDT, 24 September 1995.

During this period 7.19% of the lidar shots contained fish returns, according to our algorithm. Integrating over the depth distribution produces a density of $\sim 4.27 \times 10^{-3}$ kg m^{-2} (or 4.27 metric tons/km^2) over the surveyed habitat. We can estimate the errors introduced by noise in the lidar system by examining the returns from depths between 45 and 50 m, where no fish were observed. The average value was 1.29×10^{-5} kg m^{-3} over this depth range. This is the result of the algorithm's mistakenly identifying noise fluctuations as fish and is a bias in the technique. The standard deviation of values over this depth range was 1.01×10^{-6} kg m^{-3}. This is the random noise in the measurement.

During the next hour 1.83% of the lidar shots contained fish returns. Figure 9 shows that the habitat density is lower and the fish are now concentrated between 10 and 20 m and are starting to separate into two layers. The density for this area was 9.33×10^{-4} kg m^{-2}. The bias was 3.60×10^{-6} kg m^{-3}, and the noise was 4.97×10^{-7} kg m^{-3}. In the third hour, shown in Fig. 10, a clear separation into two layers occurred, with lower concentrations of fish from 25 to 35 m and at $\sim$40 m. The total number of fish returns during that hour was 3.20% of the number of pulses, and the average density was 1.86×10^{-3} kg m^{-2}. The bias was 6.50×10^{-6} kg m^{-3}, and the noise was 7.99×10^{-7} kg m^{-3}.

Figure 11, for 1000 to 1100 PDT, shows a thin layer of fish from $\sim$9 to 15 m, resulting from only 0.26% of the lidar pulses. The density was much lower than that recorded earlier in the morning, 1.49×10^{-4} kg m^{-2}. Because fewer pulses contribute to the signal, the bias and the noise are also lower, 5.62×10^{-7} kg m^{-3} and 1.27×10^{-7} kg m^{-3}, respectively. There is another source of error in integrated measurements of thin layers such as this. In the development up to this point we have assumed that the layers of fish are much thicker than the depth resolution of the lidar. If this is not the case, the measured profile is the convolution of the actual profile and the depth resolution of the lidar. For this case the measured full-width at half-maximum was 4.1 m. The full-width at half-maximum of the depth resolution for our 15-ns pulse is 1.6 m. The deconvolved pulse width can be estimated by the root-mean-square difference between these two, which is $\sim$3.8 m. Thus our estimate of the area density of fish over this habitat is probably too high by the ratio of 4.1 to 3.8 m or $\sim$8%. For the thicker layers of the other hours the error is less.

6. Discussion

These results demonstrate that quantitative information about fish populations can be obtained from lidar. The sampling density is determined more by cost constraints than anything else. To estimate the entire stock of fish in an area, one would sample uniformly over the area. Then the depth profiles of density would be calculated as in Figs. 8–11. The resulting density estimates could then be integrated over depth and multiplied by the surveyed area for an estimate for the total biomass within the area. While the eventual application is for an airborne system, the ship trials reported here establish the feasibility of the technique.

Clearly more work is necessary for optimal performance of such a system. It is generally straightfor-

ward for us to determine when fish are present in a lidar return, but transferring this skill to a computer is difficult. This is true especially when the water is not as homogeneous as it was during these tests. For the inhomogeneous case in particular, better ways of separating the water return from the fish return are required. We are investigating a number of techniques for improvement, including artificial neural networks trained to recognize fish schools as features within lidar signals.

Another area where more work is required is in lidar calibration. The lidar itself can be calibrated fairly accurately, although we have not done so here. The reflectivity and the conversion from area to mass depend on the species of fish and their size and age. These factors can be determined fairly accurately when the fish are shallow enough to be visible. At present, one must then assume that deeper schools in the same area have about the same composition. One can test this assumption by occasional sampling; an airborne lidar would not eliminate the need for surface survey work. The reflectivity also depends on the behavior of the fish. The individual returns during the tank measurements varied greatly, with a significant part of that variation caused by differences in the orientation of the fish within the beam. Although the average value was fairly well determined in these measurements, there may be a difference in the average for the open ocean if there are differences in behavior that affect the orientations of the fish. Note that even if the calibration issues cannot be solved satisfactorily, lidar can be used as an index of abundance, tracking relative populations over time by repeated flights over the same area.

It would also be desirable to provide quantitative values for the uncertainty of biomass estimates, which is not currently possible. The uncertainty introduced by instrument noise is easy to estimate and is fairly accurately represented by the reported values. Other sources of error are more difficult to estimate. The major error will probably arise from misidentification of targets, which depends on the characteristics of the fish, such as the school size, density, and depth. The magnitude of this error also depends both on the characteristics of other scatters in the water and the signal processing and is difficult to quantify. Further comparisons with more traditional survey techniques are required to fully quantify the performance of lidar.

This paper was generated as part of a joint National Oceanic and Atmospheric Administration (NOAA)–Department of Defense–Advanced Sensor Applications Program. We thank John Hunter and Paul Smith of NOAA Southwest Fisheries Science Center for many helpful discussions; Larry Robertson, who stocked, fed, and cared for the fish; Dan Higgins, who developed software to process lidar and video data; and the officers and crew of the R/V *David Starr Jordan*, who provided excellent support and, more importantly, found many targets for the lidar.

References

1. D. V. Holliday and H. L. Larsen, "Thickness and depth distributions of some epipelagic fish schools off Southern California," Fish. Bull. **77,** 489–494 (1979).
2. J. L. Squire Jr. and H. Krumboltz, "Profiling pelagic fish schools using airborne optical lasers and other remote sensing techniques," Mar. Technol. Soc. J. **15,** 27–31 (1981).
3. M. K. Krekova, G. M. Krekov, I. V. Samokhvalov, and V. S. Shamanaev, "Numerical evaluation of the possibilities of remote sensing of fish schools," Appl. Opt. **33,** 5715–5720 (1994).
4. D. L. Murphree, C. D. Taylor, and R. W. McClendon, "Mathematical modeling for the detection of fish by an airborne laser," AIAA J. **12,** 1686–1692 (1974).
5. K. Fredriksson, B. Galle, K. Nyström, S. Svanberg, and B. Öström, "Underwater laser-radar experiments for bathymetry and fish-school detection," Rep. No. GIPR-162 (Göteborg Institute of Physics, Göteborg, Sweden, 1978).
6. J. H. Churnside and P. A. McGillivary, "Optical properties of several Pacific fishes," Appl. Opt. **30,** 2925–2927 (1991).
7. J. A. Benigno and D. J. Kemmerer, "Aerial photographic sensing of pelagic fish schools: a comparison of two films," presented at the American Society of Photogrammetry Symposium on Remote Sensing in the Ocean, Lake Buena Vista, Fla., October 1973.
8. J. R. Hunter and J. H. Churnside, eds., "Airborne fishery assessment technology - a National Oceanic and Atmospheric Administration workshop report," SWFSC Administrative Rep. No. LJ-95-02, 1995 (Southwest Fisheries Science Center, La Jolla, Calif.), pp. 71.